Layer dependence of the electronic band alignment of few-layer MoS_2 on SiO_2 measured using photoemission electron microscopy

Morgann Berg,[1,*] Kunttal Keyshar,[2] Ismail Bilgin,[3,4] Fangze Liu,[3,4] Hisato Yamaguchi,[4] Robert Vajtai,[2] Calvin Chan,[1] Gautam Gupta,[4] Swastik Kar,[3] Pulickel Ajayan,[2] Taisuke Ohta,[1] and Aditya D. Mohite[4]

[1]*Sandia National Laboratories, Albuquerque, New Mexico, 87185, USA*

[2]*Department of Materials Science and Nanoengineering, Rice University, Houston, Texas 77005, USA*

[3]*Department of Physics, Northeastern University, Boston, Massachusetts 02115, USA*

[4]*Los Alamos National Laboratory, Los Alamos, New Mexico 87545, USA*

(Received 12 January 2017; revised manuscript received 14 April 2017; published 5 June 2017)

Tailoring band alignment layer-by-layer using heterojunctions of two-dimensional (2D) semiconductors is an attractive prospect for producing next-generation electronic and optoelectronic devices that are ultrathin, flexible, and efficient. The 2D layers of transition metal dichalcogenides (TMDs) in laboratory devices have already shown favorable characteristics for electronic and optoelectronic applications. Despite these strides, a systematic understanding of how band alignment evolves from monolayer to multilayer structures is still lacking in experimental studies, which hinders development of novel devices based on TMDs. Here, we report on the local band alignment of monolayer, bilayer, and trilayer MoS_2 on a 285-nm-thick SiO_2 substrate using an approach to probe the occupied electronic states based on photoemission electron microscopy and deep-ultraviolet light. Local measurements of the vacuum level and the valence band edge at the Brillouin zone center show that the addition of layers to monolayer MoS_2 increases the relative work function and pushes the valence band edge toward the vacuum level. We also deduced *n*-type doping of few-layer MoS_2 and type-I band alignment across monolayer-to-bilayer and bilayer-to-trilayer lateral junctions. Conducted in isolation from environmental effects owing to the vacuum condition of the measurement and an insulating SiO_2 substrate, this study shows a metrology to uncover electronic properties *intrinsic* to MoS_2 semiconducting layers and emerging 2D crystals alike.

DOI: 10.1103/PhysRevB.95.235406

I. INTRODUCTION

The design and implementation of semiconductor homo- and heterojunctions are cornerstones of today's growing electronic and optoelectronic industries. In addition to a tunable band gap and carrier control via spin and valley degrees of freedom [1–4], heterojunctions based on atomic layers of transition metal dichalcogenides (TMDs) have displayed a wide range of favorable properties in laboratory devices, well suited to electronic and optoelectronic applications [5–7]. Layered TMDs exhibit high on-off ratios in field effect devices [8–11], high photoluminescence quantum efficiency [12,13], high percentages of light absorption [14], high photogain, and photoresponse [15,16].

To obtain high performances in most of the abovementioned devices, the efficient injection of charge (or energy) across contacts and control of carrier transport across heterojunctions requires accurate determination of band alignment, including offsets of the work function, valence band maximum, and conduction band minimum. While there has been tremendous progress in the growth of TMD-based heterostructures for charge transport and optical measurements, information about their band alignment is not readily available. This is due, in part, to their electronic structures being sensitive to the number of layers and the stacking orientation [17–20]. Measurement of the band alignment has been further complicated by poor screening of interactions with the supporting substrate and physisorbed or chemisorbed gas molecules, obscuring the electronic properties intrinsic to TMD layers [21–23]. For MoS_2, a prototypical TMD, alignment of the electronic states at the junctions between layers of different thickness have been reported in studies of surface potentials typically using scanning Kelvin probe microscopy (SKPM) and electrostatic force microscopy (EFM) [24–30]. However, SKPM and EFM studies have yet to quantify the surface potential offsets at the junctions or even just to achieve a clear consensus on whether the work function rises or falls as layer number is increased. Authors have ascribed incongruous results from SKPM and EFM, often performed in ambient conditions, to hydrophilicity of the MoS_2 surface [27,31,32]. In this context, an accurate measurement of the electronic band alignment on a technologically relevant substrate, without any influence from the environment is a vital parameter for developing TMD heterostructures for novel optoelectronic devices [33,34]. The requirement for quantitative determination of the electronic band alignment *intrinsic* to few-layer TMDs also necessitates that measurements be performed on TMD specimens supported by a substrate that interacts minimally with the overlying TMDs, preferably an insulator. This condition precludes the use of electron-based spectroscopy tools, such as photoemission spectroscopy, due to the limitations imposed by sample charging. We overcome this restriction by using photoemission electron microscopy (PEEM) with deep-ultraviolet (DUV) illumination as an excitation source.

In this paper, we studied the band alignment of a model TMD system, few-layer MoS_2 supported on 285-nm-thick SiO_2 grown on a Si wafer, in an ultrahigh vacuum (UHV) environment using PEEM. Local determination of the vacuum level, valence band edge at the Brillouin zone (BZ) center, and

*Corresponding author: mberg@sandia.gov

ionization energy of monolayer (1ML), bilayer (2ML), and trilayer (3ML) MoS_2 were obtained from the local photoemission spectroscopy spectra (PES spectra) and the photon-energy-dependent photoemission yield (PEY). We observed that with the addition of layers, the vacuum level and, hence, the work function increased relative to 1ML MoS_2. The valence band edge also advanced toward the vacuum level with increasing layer number. Based on these results, we constructed a band diagram of 1ML, 2ML, and 3ML MoS_2, which shows type-I band alignment across 1ML-to-2ML and 2ML-to-3ML lateral junctions. We also determined that few-layer MoS_2 on 285-nm-thick SiO_2 is *n*-type, which we inferred from the reported work function of 1ML MoS_2 supported on a Si wafer. Our successful application of PEEM using DUV light to measure the band alignment of semiconducting TMD crystals on a nominally insulating substrate, all the while encountering minimal charging of the sample, presents insight into their electronic properties.

II. EXPERIMENTAL PROCEDURE

All MoS_2 flakes were synthesized using a slightly modified version of a well-established chemical vapor deposition (CVD) technique that proceeds via sulfurization of a MoO_2 precursor [35]. The more common CVD technique using MoO_3 was not chosen because of its tendency to grow large area 1ML with very scant 2ML nucleation [36]. Synthesis of MoS_2 with MoO_2 precursors and higher growth temperatures produced larger multilayer regions (see Supplemental Material Fig. S1 [37]) ideal for a layer-dependent PEEM study of MoS_2. The 285-nm-thick SiO_2 thermally grown on a highly-doped silicon wafer (*p*-type, 12.0–16.0 Ω cm) was chosen as a substrate material to produce optical contrast for as-grown structures [38,39]. The layer number of each MoS_2 region was verified using Raman spectroscopy (see Supplemental Material Fig. S1 [40]). To remove adsorbed water from the sample surface, samples were annealed for ∼12 h at ∼300 °C in UHV prior to PEEM measurement.

The PEEM measurements were conducted in a LEEM-III system (Elmitec Elektronenmikroskopie GmbH) coupled to a continuous-wave, tunable DUV light source comprised of a pressurized Xe lamp (Energetiq, EQ-1500 LDLS), a Czerny-Turner monochromator (Acton Research, SP2150), and refocusing optics (fused silica and calcium fluoride/silica achromatic lenses) [41]. The spectral width of the DUV light was set to 50–100 meV throughout the wavelength range used for the measurement (λ = 175–350 nm, $h\nu \cong$ 3.6–7 eV). Acquisition times for images were typically on the order of a few minutes (<5 min), and complete spectra required hours (3–18 h) to obtain. The photon flux of our tunable DUV source provided a sufficient signal-to-noise ratio of photoemission intensity to enable fitting of local PES spectra for this study. The field of view for photoemission images and spectral maps was 100 μm, with a diameter of 600 pixels, corresponding to a pixel size of ∼150 nm/pixel.

During acquisition of photoemission spectra, we used an electron filter on the LEEM-III instrument to sweep through the kinetic energies of the photoemitted electrons. No aperture restricted the emission angle of the photoelectrons. Thus, the data presented here correspond to emission-angle integrated

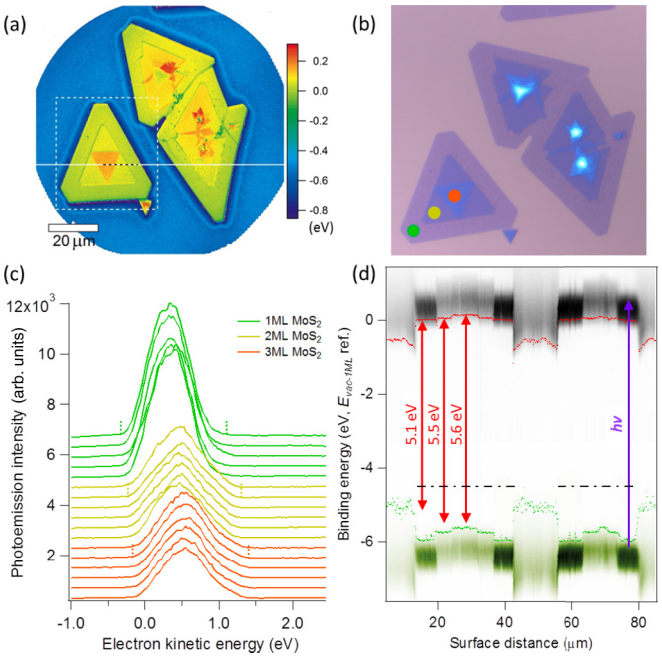

FIG. 1. The (a) vacuum level E_{vac} map, (b) the optical image, (c) the representative photoemission spectra, and (d) the alignment of the electronic states of MoS_2 flakes grown on SiO_2. (a), (c), and (d) were acquired using photons with λ = 185 nm ($h\nu$ = 6.70 eV). The color scale bar for (a) is in electron volts. The black dotted line and the white solid line in (a) illustrate the locations from which the photoemission spectra shown in (c) and (d) were obtained. In (c), the leading edges of E_{vac} (left edge) and the valence band edge (right edge) are indicated by tick marks. In (d), the alignments of E_{vac} and the valence band edges of 1ML, 2ML, and 3ML MoS_2 are indicated by the red and green dots. Superimposed images are the photoemission intensity map. The widths of superimposed photoemission intensity profiles correspond to the widths of their respective photoemission spectra. The black dash-dot lines illustrate the energy of the Fermi level deduced from the work function of 1ML MoS_2 reported in Refs. [51,52] and red bidirectional arrows represent results for the ionization energy obtained using PEY.

spectra. The leading (left) and trailing (right) edges of PES spectra yield information about the location of the vacuum level and the valence band edge at the center of the BZ, respectively [see Fig. 1(c)]. Similar to conventional analysis of x-ray photoelectron spectroscopy (XPS) and ultraviolet photoelectron spectroscopy (UPS) spectra, lines are fit to these edges and the intersects of the fitted lines with the baseline of the spectra are determined. These intersects specify the locations of the vacuum level and the valence band edge. The energy resolution of our electron energy filter was set to 0.5 eV, which results in a broadening of the PES spectral width by 0.5 eV. This broadening due to the resolution of the electron energy filter is corrected for *post facto* by shifting the leading and trailing edges of the spectra, similar to the procedure outlined in Ref. [42]. Maps of the vacuum level and the highest occupied states were obtained by fitting the PES spectra at each pixel (obtained at a fixed photon energy) and by correcting for the dispersion of the electron energy filter using a known surface (in this case, the SiO_2 background).

Local variation in the vacuum level yields the work function variation.

Ionization energy maps were obtained from PEY curves recorded at each pixel as a function of photon energy using a monochromator in tandem with our DUV light source. The electron energy filter was not used for PEY measurements. We determined ionization energy pixel-by-pixel from the minimum photon energy above which photoemission is observed (photoemission threshold) in the photon energy scan. The standard deviation of the signal acquired with lower energy photons (below the photoemission threshold) was used as a criterion to define the photoemission threshold at each pixel [43].

III. RESULTS AND DISCUSSION

The PEEM measurements and an optical image of 1ML, 2ML, and 3ML MoS_2 grown on 285-nm-thick SiO_2 are shown in Fig. 1. The data in Figs. 1(a), 1(c), and 1(d) were acquired using photons with $\lambda = 185$ nm (6.70 eV). Figure 1(a) shows the vacuum level map, where the relative vacuum levels E_{vac} of 1ML, 2ML, 3ML, and multilayer MoS_2, as well as that of the SiO_2 substrate are clearly distinguishable. The vacuum level of the SiO_2 substrate lies ~0.5 eV lower in energy than that of 1ML MoS_2. The thickness of the MoS_2 flakes is verified from the optical contrast shown in Fig. 1(b) and is further confirmed from the Raman spectra at the locations highlighted by the green, yellow, and orange dots corresponding to 1ML, 2ML, and 3ML (see Supplemental Material Fig. S1 [40]). The crystallographic alignment between layers can be inferred from the relative orientations of the triangular edges [44]. Most flakes display $2H$ or $3R$ stacking with random stacking orientation for thicker parts of the flakes [45].

Figure 1(c) shows representative PES spectra for 1ML, 2ML, and 3ML regions indicated by the black dotted line in Fig. 1(a). The leading (left) edge and trailing (right) edge of PES spectra, which yield information about the location of E_{vac} and valence band edge at the center of the BZ, are indicated by tick marks in Fig. 1(c). With increasing layer number, E_{vac} (left edge of the peak in PES spectra) and the valence band edge (right edge of the peak in PES spectra) are shifted higher in kinetic energy for MoS_2. The variation of the local E_{vac} shown in Figs. 1(a) and 1(c) establishes a layer-dependent surface potential in MoS_2. In Fig. 1(c), the PES intensity from 1ML MoS_2 appears higher than that of 2ML and 3ML MoS_2. Note that the relative intensities between MoS_2 regions with different thicknesses varied as function of photon energy. We postulate that this enhancement of the photoemission intensity results from the difference of the photoemission cross section for different thicknesses of MoS_2 at the particular photon energy used in the measurement [46–49].

Combining information concerning E_{vac}, the valence band edge, and the photon energy enables us to examine the alignment of the electronic states across 1ML, 2ML, and 3ML MoS_2. The PES spectra at each pixel along the white line in Fig. 1(a) were extracted and are presented as surface band alignment in Fig. 1(d). Higher photoemission intensities appear darker in color. The green photoemission intensity map represents the initial filled state, which is inferred by offsetting the black PES spectra by the photon energy used for the PES measurement ($\lambda = 185$ nm or $h\nu = 6.70$ eV). The energy of the valence band edge is thereby expressed in terms of the electron binding energy with respect to the vacuum level of 1ML MoS_2 by considering the following relationship:

$$(BE_{rel})_{1ML\ MoS_2} = (KE_{rel})_{1ML\ MoS_2} - h\nu,$$

where $(BE_{rel})_{1ML\ MoS_2}$ and $(KE_{rel})_{1ML\ MoS_2}$ are the binding energy and the kinetic energy relative to 1ML MoS_2, respectively. This difference in binding energy between the vacuum level and valence band edge at the BZ center is the ionization energy as measured using PES. Because we use low-energy photons in our measurement, the highest occupied states measured reflect the valence band edge near the Γ point.

The vacuum level alignment is presented via red dots in Fig. 1(d). These values were extracted from the leading edge of the PES spectra [the left edge in Fig. 1(c)] shifted 0.25 eV higher in electron kinetic energy (i.e., toward the right edge) to account for energy broadening due to the moderate electron energy resolution of the measurement (~0.5 eV). The alignment of the valence band edge at BZ center is presented in green dots, whose values were extracted from the trailing edge of the PES spectra [the right edge in Fig. 1(c)]. Again, the trailing edge of the PES spectra was shifted to lower kinetic energy by 0.25 eV to account for energy broadening. The magnitude of the ionization energies for 1ML, 2ML, and 3ML MoS_2 that were determined from the PEY map (see Supplemental Material Fig. S2 [50]) are represented by red arrows in Fig. 1(d). Ionization energy measurements are obtained from PEY spectra by analyzing the threshold energy of illumination at which photoemission occurs. For metals, this threshold energy corresponds to the work function of the metal, while for a semiconductor lacking states at the Fermi level, this threshold energy corresponds to the ionization energy—the difference in energy between the vacuum level and valence band edge.

Assuming a 4.49 eV work function for 1ML MoS_2 [51,52] and that the Fermi level is aligned between 1ML, 2ML, and 3ML MoS_2 within a single crystalline flake, the location of the Fermi level is shown by the black dash-dot lines illustrated in Fig. 1(d). The latter assumption is reasonable given a lack of chemical bonding between MoS_2 and the underlying SiO_2 [11], and the van der Waals interlayer coupling between MoS_2 layers [53]. References [51,52] measured work function values for 1ML MoS_2 specimens (4.49 and 4.52 eV, respectively) that received little exposure to ambient conditions and were annealed in inert environments, consistent with the conditions of our measurement. Further assuming that the optical band gap values of 1ML, 2ML, and 3ML MoS_2 are ~1.9,~1.6, and ~1.4 eV [17], our experimental data suggest that the Fermi level of the MoS_2 flake is above midgap, indicating n-type character. This result is consistent with the n-type conductivity commonly found in 1ML MoS_2 on SiO_2 and bulk $2H$-MoS_2 [54,55]. Another important aspect of Fig. 1(d) is the abrupt transitions of both E_{vac} and the valence band edge at the junctions between MoS_2 regions of different thicknesses. Band bending at the heterojunctions between TMDs with different layer numbers has been observed but at the nanometer scale [34]. Figure 1(d) confirms that such band bending is absent at the larger length scale probed in

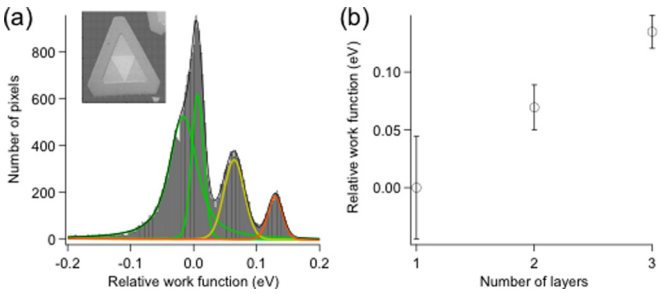

FIG. 2. Determination of the work function variation in a MoS_2 flake. (a) Histogram of E_{vac} obtained for the imaged MoS_2 island shown in the inset. (b) The relative work function of 1ML, 2ML, and 3ML MoS_2. The error bars in the relative work function are the widths of the fitted peaks in (a). Incomplete removal of the dispersion background necessitated that the relative work function distribution of 1ML MoS_2 be fit with two components shown in green. Thus, the error bar in Fig. 2(b) for 1ML MoS_2 corresponds to the FWHM of the overall fit composed of the superposition of the two green peaks.

the present PEEM experiment. Further details of the band alignment are discussed in the following.

From Fig. 1(d), it appears that the ionization energy we measured from PEY (see Supplemental Material Fig. S2 [50]) (red arrows) and the ionization energy we deduced from the PES spectra (green dots) do not agree for 1ML and 2ML MoS_2, deviating significantly ($\sim$0.9 eV) for 1ML MoS_2. In contrast, they show reasonable agreement for 3ML MoS_2. These discrepancies in 1ML and 2ML MoS_2, we believe, are largely due to the photoemission signal of the underlying SiO_2 substrate. Figure 1(d) shows that the measured ionization energy of SiO_2 is lower than that of MoS_2. Therefore, we expect the PEY intensity of the MoS_2 flakes at the lower photon energy (longer wavelength) range would be overwhelmed by the photoelectrons from SiO_2. Furthermore, a general trend of a longer probing depth with longer wavelength photons could increase the relative contribution of the underlying SiO_2 in the photoemission intensity [56]. This scenario is supported by PES spectra acquired for photons with $\lambda = 200$ nm, where additional spectral weight from the SiO_2 substrate is visible in the PES spectra, beyond that of MoS_2 (see Supplemental Material Fig. S3(a) [57]). We note that 1ML and 2ML MoS_2 show larger additional spectral weights than does 3ML, in which the SiO_2 signal is mostly attenuated. Overall, reasonable agreement of the ionization energy of 3ML MoS_2 evaluated from the PES and PEY measurements supports the validity of the energy scale used in our analysis. Because results from PES spectra for MoS_2 are reliable regardless of the MoS_2 thickness, we continue our discussion of the band alignment based on the PES data taken with higher-energy photons ($\lambda = 185$ nm).

Clear distinction between 1ML, 2ML, and 3ML regions in the E_{vac} map in Fig. 1(a) allows for quantifying variation in the local work function. The histogram of the extracted E_{vac} values and the plot of relative work function are presented in Figs. 2(a) and 2(b). We fit the E_{vac} distribution in Fig. 2(a) with Voigt functions. The full width at half maximum (FWHM) of each fit component corresponds to the error in relative work function values plotted in Fig. 2(b). We note that because our PES measurements using PEEM do not have an absolute energy scale, the E_{vac} measurements are reported relative to that of 1ML MoS_2.

From Fig. 2(b), we found that the relative work function increases by $\sim$70 meV with each additional MoS_2 layer. Thus, if the work function of 1ML MoS_2 is 4.49 eV [51,52], our results suggest that those of 2ML and 3ML MoS_2 are 4.55 and 4.63 eV, respectively. The trend of work function increase with increasing number of layers has not been established among SKPM and EFM studies of MoS_2. Both increasing and decreasing work function with increasing layer number have been reported. One may surmise that hydrophilicity of MoS_2 and the effects of ambient conditions account for this inconsistency [27]. We also note that to arrive at surface potentials, SKPM uses the capacitive difference between a conducting AFM probe and a charge layer thickness in the sample. For semiconducting crystals suspended on substrates, it is not clear to what extent charge layers in the substrate may contribute to stray fields and whether the substrate and sample have reached thermodynamic equilibrium [58]. Both can influence SKPM results. To our knowledge, the only SKPM study to observe work function variation similar to what we observed in the present paper was conducted in UHV (the work function increases by $\sim$50 meV with each additional MoS_2 layer) [52]. This appears to confirm that the work function increase as a function of the layer number we observed reflects the electronic properties of MoS_2 flakes supported on an insulating substrate, minimally perturbed by environmental effects (thanks to UHV conditions).

Based on the measured variations of the relative work function and valence band edge at the Γ point of MoS_2, we determine the band alignments across 1ML, 2ML, and 3ML. Figure 3 shows a simplified schematic of the band alignment between MoS_2 and SiO_2. The schematic includes reported band gap values for 1ML, 2ML, and 3ML MoS_2 [54], as well as the energy differences of the valence band edges at the Γ point versus the K point ($\Delta E_{\Gamma\text{-}K}$) based on theoretical calculations (Ref. [59] for 1ML and 2ML and Ref. [60] for 3ML). Also shown in Fig. 3 is the position of the Fermi level deduced from the 4.49 eV work function for 1ML MoS_2 reported in Refs. [51,52].

As a whole, Fig. 3 points to some important aspects of the junctions between 1ML, 2ML, and 3ML MoS_2. First, the Fermi levels of the MoS_2 lie a few 100 meV above midgap in all three thicknesses, as described earlier. Because of the similar effective electron and hole masses for 1ML MoS_2 ($m^*_e = 0.54$ and $m^*_h = 0.44$) [61], we can expect that the Fermi level of the intrinsic 1ML MoS_2 would lie close to the midgap. This scenario suggests the n-type character of 1ML MoS_2 grown on SiO_2. As the effective electron and hole masses are similar for 2ML and 3ML, they are expected to be n-type as well. The band diagram also suggests type-I band alignment across the 1ML–2ML and 2ML–3ML heterojunctions. This result is in a qualitative agreement with the theoretical calculations by Padilha *et al.* [60] and Kang *et al.* [62] and contradicts a scanning photocurrent microscopy study, which suggests a type-II heterojunction between 1ML and multilayer MoS_2 on SiO_2 [63].

One uncertainty in the band diagram (Fig. 3) is the difference in energy of the valence band edges at the Γ point versus the K point ($\Delta E_{\Gamma\text{-}K}$) in 1ML MoS_2. While we use

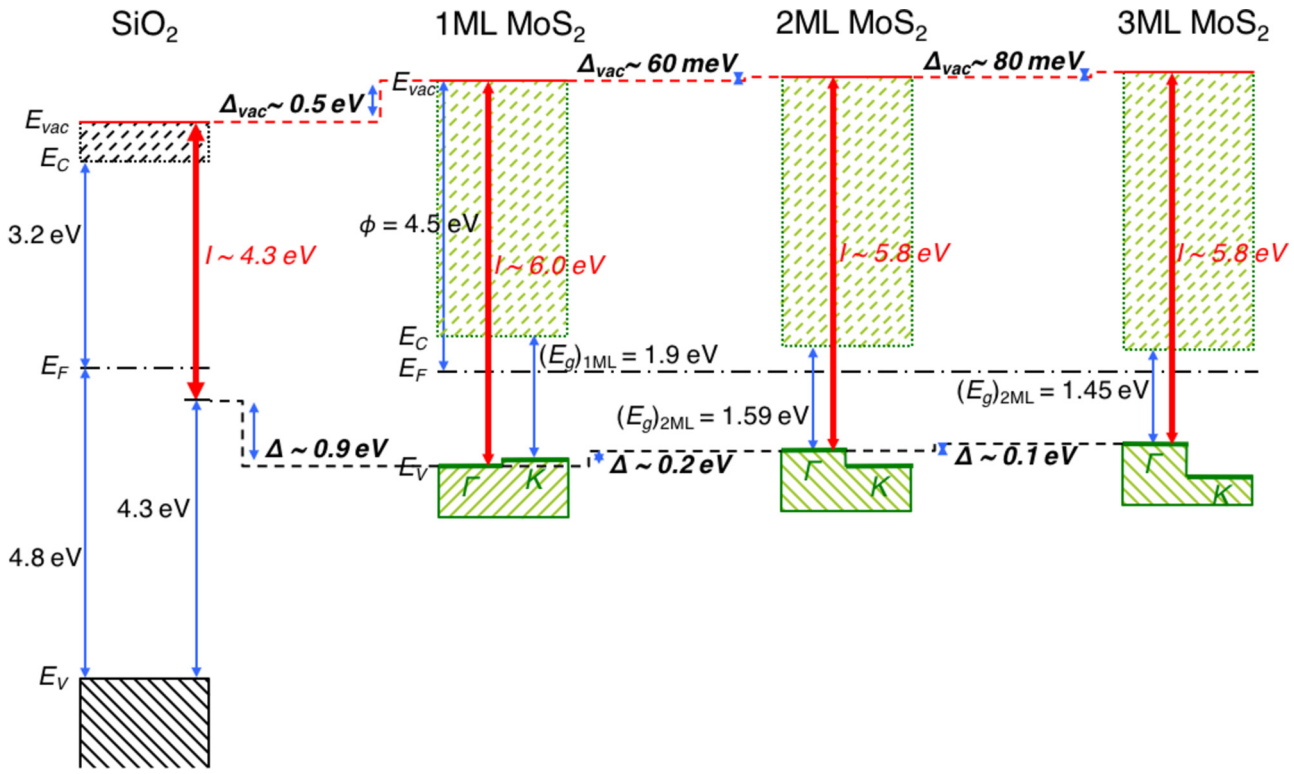

FIG. 3. A simplified band diagram of 1ML, 2ML, and 3ML MoS_2 and SiO_2, which includes quantities measured with PEEM in boldfaced, italicized type. The ionization energies were calculated from PES spectra and are represented with red arrows and fonts. Other numbers are based on the reported values, as described in the main text.

$\Delta E_{\Gamma\text{-}K} = 0.1$ eV based on a theoretical work [59], an angle resolved photoemission spectroscopy (ARPES) measurement of 1ML MoS_2 on Au(111) suggests $\Delta E_{\Gamma\text{-}K}$ as large as 0.3 eV [64,65]. Were this so, it would imply that band alignment across the 1ML–2ML MoS_2 heterojunction is type II. Because ARPES measurements of 1ML MoS_2 on less interacting substrates (thin SiO_2/Si [66] and graphene/SiC [49]) suggest $\Delta E_{\Gamma\text{-}K} = 0.1$ eV, we presume $\Delta E_{\Gamma\text{-}K} = 0.1$ eV for 1ML MoS_2 on thick SiO_2. Accordingly, a type-I heterojunction is expected at the 1ML–2ML MoS_2 interface formed on SiO_2. We speculate that the type-II heterojunction found in the scanning photocurrent microscopy study may be the result of light-induced defects or trapped charges at the surface of SiO_2 influencing the band alignment of MoS_2. Further study is needed to gain a comprehensive understanding of the influence of trapped charge. We also note that even $\Delta E_{\Gamma\text{-}K} = 0.3$ eV does not alter our assessment of n-type character for 1ML MoS_2.

Additional uncertainty in the band diagram arises due to twist angles between layers and stacking sequence. Though we did not characterize the stacking configuration of our sample, we note that triangular flakes in our sample adopted angles of either 0° or 60° relative to one another [Fig. 1(c)]. Theory suggests that is indicative of either of two stable stacking configurations, $2H(AA')$ or $3R(AB)$ [67,68]. A recent μ-ARPES study of twisted 2ML MoS_2 on native oxide layers on Si [69] demonstrates that a twist angle of 60° ($2H$ or AA' stacking) relative to the $3R(AB)$ configuration shifts the Γ point downward in energy by as much as 40 meV, while the K point appears largely unaffected by twist angles ranging from 0° ($3R$ or AB stacking) to 60° ($2H$ or AA' stacking). Such a shift in energy of the Γ point would not significantly impact the type-I band alignment we observe across the 1ML–2ML MoS_2 heterojunction, nor alter our assessment of n-type MoS_2.

Figure 3 provides electronic structure information for SiO_2 in addition to that for MoS_2. From Fig. 1(d), E_{vac} of SiO_2 is located at 0.5 eV below that of 1ML MoS_2, while the highest occupied state in SiO_2 lies at −4.8 eV binding energy (with respect to the E_{vac} of 1ML MoS_2). Figure 3 also shows an 8.0 eV band gap and 8.6 eV ionization energy for SiO_2 and a Fermi level that sits above midgap (4.8 eV above the valence band of SiO_2) based on previous reports [70,71]. There is type-I band alignment across the lateral MoS_2-SiO_2 heterojunction for which we expect minimal band bending owing to van der Waals interactions between MoS_2 and the substrate. We note that the 4.3 eV energy difference between E_{vac} and the highest occupied state in SiO_2 is significantly smaller than the expected ionization energy of SiO_2 (8.6 eV) [71].

We postulate the highest occupied state shown in the PES spectra from SiO_2 [Fig. 1(d)] corresponds to defects in SiO_2. From photoluminescence studies, oxygen deficiency centers (ODCs) [72] have been shown to produce emission bands 4.3 eV above the valence band of SiO_2 [73–76]. Defects in SiO_2 are also observed in the DUV photoemission spectra of glassy SiO_2 and quartz implanted with metals ions [77,78]. In Fig. 3, the highest occupied state probed in our experiment [see Fig. 1(d)] is located at 4.3 eV below the vacuum level of SiO_2 and coincides well with an energy level of ODCs. Over the course of our PES measurements, we observed the

photoemission intensity from the SiO_2 substrate to vary as a function of the photon wavelength in a manner consistent with the photoemission intensity variation reported in Refs. [77,78].

Photoemission experiments on insulating materials are generally not reported because of sample charging, which obscures the interpretation of the spectra or image. In this regard, this paper presents the case where photoemission microscopy and spectroscopy can be performed on MoS_2 flakes supported on nominally insulating 285-nm-thick SiO_2. Similar PEEM measurements of 2D crystals on thick SiO_2 are reported, but they were conducted with the aid of additional grounding [79,80] or alkali metal doping [81] to alleviate charging. Furthermore, PEEM imaging of an insulator surface free of image distortion or charging was once demonstrated on a SiO_2 film using a supplemental electron source in addition to the uv illumination [82]. These works suggest that PEEM of 2D semiconducting layers supported by insulating substrates is possible, provided there are means to compensate for charge accumulation at the sample surface.

To verify that the PES spectra presented here are minimally influenced by charging, we recorded PES spectra as a function of photon energy, and confirmed that the spectral width increases linearly with a slope close to unity (see Supplemental Material Fig. S3(b) [83]). This result confirms that there is no additional elongation of the spectral width as a function of the photon energy, which is one signature of sample charging. We attribute the apparent absence of charging to two factors: the low photoelectron current of our measurement technique and the dissipation of photoholes responsible for surface charging by photoactive defects in SiO_2 moving charges to and from the MoS_2 flakes. We note that illumination of a similar sample using a He discharge lamp ($h\nu = 21.2$ eV) resulted in instant charging, likely because of the higher photoelectron current produced at the higher excitation energy. Further experimental verification of the charging behavior of MoS_2 flakes on SiO_2 using a He lamp is provided in Supplemental Material Fig. S3(b) [83].

Electron spectroscopy is a powerful tool for studying electronic properties of materials, but it is generally limited to conductive materials. This limitation has hampered the study of electronic properties intrinsic to 2D crystals supported on insulating substrates in order to minimize electronic perturbation. The paper presented here resolves this quandary for 2D crystals research and suggests that this approach based on PEEM and DUV illumination may be used to study the electronic properties intrinsic to other 2D crystals supported on SiO_2.

IV. CONCLUSION

In summary, a study of the electronic state alignment in 1ML, 2ML, and 3ML MoS_2 on a 285-nm-thick SiO_2 substrate has been presented. The layer dependence of the photoemission spectra showed a trend of increasing work function and shifting of the valence band edge at BZ center toward the vacuum level with increasing layer thickness. Based on our measurements, we proposed the band alignment between MoS_2 layers. We deduced that MoS_2 is n-type and showed type-I band alignment across 1ML-to-2ML and 2ML-to-3ML lateral junctions. Our results demonstrate that PEEM coupled to a DUV light source is a powerful tool to evaluate the electronic properties of MoS_2 with minimal environmental influence and can be employed to study other 2D layered semiconductors and metals. The band alignment derived in the present paper is essential information for building electronic and optoelectronic devices based on atomically thin MoS_2.

ACKNOWLEDGMENTS

We thank R. Guild Copeland for his help in constructing the tunable DUV light source. We also thank P. J. Feibelman for fruitful discussions. The photoemission electron microscopy work was performed at the Center for Integrated Nanotechnologies (CINT), a U.S. Department of Energy Office of Science User Facility (Grant No. DE-AC04-94AL85000). The work performed by M.B. and C.C. is supported by a U.S. Department of Energy, Office of Energy Efficiency and Renewable Energy SunShot Initiative award for Bridging Research Interactions through Collaborative Development Grants in Energy (BRIDGE, Award No. DE-FOA-0000654 CPS25859). K.K. was supported by the Army Research Office Multidisciplinary University Research Initiative (Grant No. W911NF-11-1-0362). S.K. acknowledges partial financial support from the National Science Foundation (Grant No. ECCS 1351424) and a Northeastern University Provost's Tier-1 Seed Grant. T.O. is supported by the CINT user program and Sandia Laboratory Directed Research & Development (LDRD). A.D.M. is supported by the Los Alamos National Laboratory LDRD program. Sandia National Laboratories is a multi-mission laboratory managed and operated by National Technology and Engineering Solutions of Sandia, LLC., a wholly owned subsidiary of Honeywell International, Inc., for the U.S. Department of Energy's National Nuclear Security Administration under Contract No. DE-NA0003525.

[1] A. K. Geim and I. V. Grigorieva, Van der Waals heterostructures, Nature (London) **499**, 419 (2013).

[2] D. Xiao, G.-B. Liu, W. Feng, X. Xu, and W. Yao, Coupled Spin and Valley Physics in Monolayers of MoS_2 and Other Group-VI Dichalcogenides, Phys. Rev. Lett. **108**, 196802 (2012).

[3] C. Huang, S. Wu, A. M. Sanchez, J. J. P. Peters, R. Beanland, J. S. Ross, P. Rivera, W. Yao, D. H. Cobden, and X. Xu, Lateral heterojunctions within monolayer $MoSe_2$-WSe_2 semiconductors, Nat. Mater. **13**, 1096 (2014).

[4] K. F. Mak, K. L. McGill, J. Park, and P. L. McEuen, The valley Hall effect in MoS_2 transistors, Science **344**, 1489 (2014).

[5] B. Radisavljevic, M. B. Whitwick, and A. Kis, Integrated circuits and logic operations based on single-layer MoS_2, ACS Nano **5**, 9934 (2011).

[6] H. Wang, L. Yu, Y.-H. Lee, Y. Shi, A. Hsu, M. L. Chin, L.-J. Li, M. Dubey, J. Kong, and T. Palacios, Integrated circuits based on bilayer MoS_2 transistors, Nano Lett. **12**, 4674 (2012).

[7] Z. Yin, H. Li, H. Li, L. Jiang, Y. Shi, Y. Sun, G. Lu, Q. Zhang, X. Chen, and H. Zhang, Single-layer MoS_2 phototransistors, ACS Nano **6**, 74 (2012).

[8] V. Podzorov, M. E. Gershenson, Ch. Kloc, R. Zeis, and E. Bucher, High-mobility field-effect transistors based on transition metal dichalcogenides, Appl. Phys. Lett. **84**, 3301 (2004).

[9] K. S. Novoselov, D. Jiang, F. Schedin, T. J. Booth, V. V. Khotkevich, S. V. Morozov, and A. K. Geim, Two-dimensional atomic crystals, Proc. Natl. Acad. Sci. USA **102**, 10451 (2005).

[10] R. Fivaz and E. Mooser, Mobility of charge carriers in semiconducting layer structures, Phys. Rev. **163**, 743 (1967).

[11] B. Radisavljevic, A. Radenovic, J. Brivio, V. Giacometti, and A. Kis, Single-layer MoS_2 transistors, Nat. Nanotechnol. **6**, 147 (2011).

[12] A. Splendiani, L. Sun, Y. Zhang, T. Li, J. Kim, C.-Y. Chim, G. Galli, and F. Wang, Emerging photoluminescence in monolayer MoS_2, Nano Lett. **10**, 1271 (2010).

[13] M. Amani, D.-H. Lien, D. Kiriya, J. Xiao, A. Azcatl, J. Noh, S. R. Madhvapathy, R. Addou, S. KC, M. Dubey, K. Cho, R. M. Wallace, S.-C. Lee, J.-H. He, J. W. Ager, III, X. Zhang, E. Yablonovitch, and A. Javey, Near-unity photoluminescence quantum yield in MoS_2, Science **350**, 1065 (2015).

[14] M. Bernardi, M. Palummo, and J. C. Grossman, Extraordinary sunlight absorption and one nanometer thick photovoltaics using two-dimensional monolayer materials, Nano Lett. **13**, 3664 (2013).

[15] D.-S. Tsai, K.-K. Liu, D.-H. Lien, M.-L. Tsai, C.-F. Kang, C.-A. Lin, L.-J. Li, and J.-H. He, Few-layer MoS_2 with high broadband photogain and fast optical switching for use in harsh environments, ACS Nano **7**, 3905 (2013).

[16] W. Zhang, J.-K. Huang, C.-H. Chen, Y.-H. Chang, Y.-J. Cheng, and L.-J. Li, High-gain phototransistors based on a CVD MoS_2 monolayer, Adv. Mater. **25**, 3456 (2013).

[17] K. F. Mak, C. Lee, J. Hone, J. Shan, and T. F. Heinz, Atomically Thin MoS_2: A New Direct-Gap Semiconductor, Phys. Rev. Lett. **105**, 136805 (2010).

[18] S. Huang, X. Ling, L. Liang, J. Kong, H. Terrones, V. Meunier, and M. S. Dresselhaus, Probing the interlayer coupling of twisted bilayer MoS_2 using photoluminescence spectroscopy, Nano Lett. **14**, 5500 (2014).

[19] A. M. van der Zande, J. Kunstmann, A. Chernikov, D. A. Chenet, Y. You, X. Zhang, P. Y. Huang, T. C. Berkelbach, L. Wang, F. Zhang, M. S. Hybertsen, D. A. Muller, D. R. Reichman, T. F. Heinz, and J. C. Hone, Tailoring the electronic structure in bilayer molybdenum disulfide via interlayer twist, Nano Lett. **14**, 3869 (2014).

[20] K. Liu, L. Zhang, T. Cao, C. Jin, D. Qiu, Q. Zhou, A. Zettl, P. Yang, S. G. Louie, and F. Wang, Evolution of interlayer coupling in twisted molybdenum disulfide bilayers, Nat. Commun. **5**, 4966 (2014).

[21] C. Hwang, D. A. Siegel, S.-K. Mo, W. Regan, A. Ismach, Y. Zhang, A. Zettl, and A. Lanzara, Fermi velocity engineering in graphene by substrate modification, Sci. Rep. **2**, 590 (2012).

[22] D. P. DiVincenzo and E. J. Mele, Self-consistent effective-mass theory for intralayer screening in graphite intercalation compounds, Phys. Rev. B **29**, 1685 (1984).

[23] J. H. Kim, J. Lee, J. H. Kim, C. C. Hwang, C. Lee, and J. Y. Park, Work function variation of MoS_2 atomic layers grown with chemical vapor deposition: The effects of thickness and the adsorption of water/oxygen molecules, Appl. Phys. Lett. **106**, 251606 (2015).

[24] B. J. Robinson, C. E. Giusca, Y. T. Gonzalez, N. D. Kay, O. Kazakova, and O. V. Kolosov, Structural, optical and electrostatic properties of single and few-layers MoS_2: Effect of substrate, 2D Mater. **2**, 015005 (2015).

[25] M. Tosun, D. Fu, S. B. Desai, C. Ko, J. S. Kang, D.-H. Lien, M. Najmzadeh, S. Tongay, J. Wu, and A. Javey, MoS_2 heterojunctions by thickness modulation, Sci. Rep. **5**, 10990 (2015).

[26] V. Kaushik, D. Varandani, and B. R. Mehta, Nanoscale mapping of layer-dependent surface potential and junction properties of CVD-grown MoS_2 domains, J. Phys. Chem. C **119**, 20136 (2015).

[27] Y. Li, C.-Y. Xu, and L. Zhen, Surface potential and interlayer screening effects of few-layer MoS_2 nanoflakes, Appl. Phys. Lett. **102**, 143110 (2013).

[28] S.-H. Choi, Z. Shaolin, and W. Yang, Layer-number-dependent work function of MoS_2 nanoflakes, J. Korean Phys. Soc. **64**, 1550 (2014).

[29] A. Castellanos-Gomez, E. Cappelluti, R. Roldán, N. Agraït, F. Guinea, and G. Rubio-Bollinger, Electric-field screening in atomically thin layers of MoS_2: The role of interlayer coupling, Adv. Mater. **25**, 899 (2013).

[30] G. Hao, Z. Huang, Y. Liu, X. Qi, L. Ren, X. Peng, L. Yang, X. Wei, and J. Zhong, Electrostatic properties of few-layer MoS_2 films, AIP Adv. **3**, 042125 (2013).

[31] M. Chhowalla, and G. A. J. Amaratunga, Thin films of fullerene-like MoS_2 nanoparticles with ultra-low friction and wear, Nature (London) **407**, 164 (2000).

[32] Y. Li, C.-Y. Xu, P. Hu, and L. Zhen, Carrier control of MoS_2 nanoflakes by functional self-assembled monolayers, ACS Nano **7**, 7795 (2013).

[33] N. R. Wilson, P. V. Nguyen, K. L. Seyler, P. Rivera, A. J. Marsden, Z. P. L. Laker, G. C. Constantinescu, V. Kandyba, A. Barinov, N. D. M. Hine, X. Xu, and D. H. Cobden, Band parameters and hybridization in 2D semiconductor heterostructures from photoemission spectroscopy, arXiv:1601.05865.

[34] C. Zhang, Y. Chen, J.-K. Huang, X. Wu, L.-J. Li, W. Yao, J. Tersoff, and C.-K. Shih, Visualizing band offsets and edge states in bilayer–monolayer transition metal dichalcogenides lateral heterojunction, Nat. Commun. **7**, 10349 (2016).

[35] I. Bilgin, F. Liu, A. Vargas, A. Winchester, M. K. L. Man, M. Upmanyu, K. M. Dani, G. Gupta, S. Talapatra, A. D. Mohite, and S. Kar, Chemical vapor deposition synthesized atomically thin molybdenum disulfide with optoelectronic-grade crystalline quality, ACS Nano **9**, 8822 (2015).

[36] Y.-H. Lee, X.-Q. Zhang, W. Zhang, M.-T. Chang, C.-T. Lin, K.-D. Chang, Y.-C. Yu, J. T.-W. Wang, C.-S. Chang, L.-J. Li, and T.-W. Lin, Synthesis of large-area MoS_2 atomic layers with chemical vapor deposition, Adv. Mater. **24**, 2320 (2012).

[37] See Supplemental Material at http://link.aps.org/supplemental/10.1103/PhysRevB.95.235406 for further details of the growth method in Fig. S1.

[38] M. M. Benameur, B. Radisavljevic, J. S. Héron, S. Sahoo, H. Berger, and A. Kis, Visibility of dichalcogenide nanolayers, Nanotechnology **22**, 125706 (2011).

[39] P. Blake, E. W. Hill, A. H. Castro Neto, K. S. Novoselov, D. Jiang, R. Yang, T. J. Booth, and A. K. Geim, Making graphene visible, Appl. Phys. Lett. **91**, 063124 (2007).

[40] See Supplemental Material at http://link.aps.org/supplemental/10.1103/PhysRevB.95.235406 for details of Raman characterization in Fig. S1.

[41] J. W. Harter, P. D. C. King, E. J. Monkman, D. E. Shai, Y. Nie, M. Uchida, B. Burganov, S. Chatterjee, and K. M. Shen, A tunable

low-energy photon source for high-resolution angle-resolved photoemission spectroscopy, Rev. Sci. Instrum. **83**, 113103 (2012).

[42] Y. Yi, J. E. Lyon, M. M. Beerbom, and R. Schlaf, Characterization of indium tin oxide surfaces and interfaces using low intensity x-ray photoemission spectroscopy, J. Appl. Phys. **100**, 093719 (2006).

[43] M. M. Ugeda, A. J. Bradley, S.-F. Shi, F. H. da Jornada, Y. Zhang, D. Y. Qiu, W. Ruan, S.-K. Mo, Z. Hussain, Z.-X. Shen, F. Wang, S. G. Louie, and M. F. Crommie, Giant bandgap renormalization and excitonic effects in a monolayer transition metal dichalcogenide semiconductor, Nat. Mater. **13**, 1091 (2014).

[44] Y. Gong, J. Lin, X. Wang, G. Shi, S. Lei, Z. Lin, X. Zou, G. Ye, R. Vajtai, B. I. Yakobson, H. Terrones, M. Terrones, B. K. Tay, J. Lou, S. T. Pantelides, Z. Liu, W. Zhou, and P. M. Ajayan, Vertical and in-plane heterostructures from WS_2/MoS_2 monolayers, Nat. Mater. **13**, 1135 (2014).

[45] J. Yan, J. Xia, X. Wang, L. Liu, J.-L. Kuo, B. K. Tay, S. Chen, W. Zhou, Z. Liu, and Z. X. Shen, Stacking-dependent interlayer coupling in trilayer MoS_2 with broken inversion symmetry, Nano Lett. **15**, 8155 (2015).

[46] R. H. Williams and A. J. McEvoy, Photoemission studies of MoS_2, Phys. Status Solidi **47**, 217 (1971).

[47] J. C. McMenamin and W. E. Spicer, Photoemission studies of layered transition-metal dichalcogenides: MoS_2, Phys. Rev. B **16**, 5474 (1977).

[48] T. Ohta, A. Bostwick, J. L. McChesney, T. Seyller, K. Horn, and E. Rotenberg, Interlayer Interaction and Electronic Screening in Multilayer Graphene Investigated with Angle-Resolved Photoemission Spectroscop *y*, Phys. Rev. Lett. **98**, 206802 (2007).

[49] J. A. Miwa, M. Dendzik, S. S. Grønborg, M. Bianchi, J. V. Lauritsen, P. Hofmann, and S. Ulstrup, Van der Waals epitaxy of two-dimensional MoS_2—Graphene heterostructures in ultrahigh vacuum, ACS Nano **9**, 6502 (2015).

[50] See Supplemental Material at http://link.aps.org/supplemental/10.1103/PhysRevB.95.235406 for further details of the PEY map in Fig. S2.

[51] J.-M. Yun, Y.-J. Noh, J.-S. Yeo, Y.-J. Go, S.-I. Na, H.-G. Jeong, J. Kim, S. Lee, S.-S. Kim, H. Y. Koo, T.-W. Kim, and D.-Y. Kim, Efficient work-function engineering of solution-processed MoS_2 thin-films for novel hole and electron transport layers leading to high-performance polymer solar cells, J. Mater. Chem. C **1**, 3777 (2013).

[52] O. Ochedowski, K. Marinov, N. Scheuschner, A. Poloczek, B. K. Bussmann, J. Maultzsch, and M. Schleberger, Effect of contaminations and surface preparation on the work function of single layer MoS_2, Beilstein J. Nanotechnol. **5**, 291 (2014).

[53] A. Koma, Van der Waals epitaxy—A new epitaxial growth method for a highly lattice-mismatched system, Thin Solid Films **216**, 72 (1992).

[54] A. Ayari, E. Cobas, O. Ogundadegbe, and M. S. Fuhrer, Realization and electrical characterization of ultrathin crystals of layered transition-metal dichalcogenides, J. Appl. Phys. **101**, 014507 (2007).

[55] S. Ghatak, A. N. Pal, and A. Ghosh, Nature of electronic states in atomically thin MoS_2 field-effect transistors, ACS Nano **5**, 7707 (2011).

[56] M. P. Seah, and W. A. Dench, Quantitative electron spectroscopy of surfaces: A standard data base for wlectron inelastic mean free paths in solids, Surf. Interface Anal. **1**, 2 (1979).

[57] See Supplemental Material at http://link.aps.org/supplemental/10.1103/PhysRevB.95.235406 for substrate contributions to the PES spectra of MoS_2 for photons with $\lambda = 200$ nm in Fig. S3(a).

[58] N. Koch, C. Chan, A. Kahn, and J. Schwartz, Lack of thermodynamic equilibrium in conjugated organic molecular thin films, Phys. Rev. B **67**, 195330 (2003).

[59] K. Kośmider and J. Fernández-Rossier, Electronic properties of the MoS_2-WS_2 heterojunction, Phys. Rev. B **87**, 075451 (2013).

[60] J. E. Padilha, H. Peelaers, A. Janotti, and C. G. Van de Walle, Nature and evolution of the band-edge states in MoS_2: From monolayer to bulk, Phys. Rev. B **90**, 205420 (2014).

[61] E. S. Kadantsev and P. Hawrylak, Electronic structure of a single MoS_2 monolayer, Solid State Commun. **152**, 909 (2012).

[62] J. Kang, S. Tongay, J. Zhou, J. Li, and J. Wu, Band offsets and heterostructures of two-dimensional semiconductors, Appl. Phys. Lett. **102**, 012111 (2013).

[63] S. L. Howell, D. Jariwala, C.-C. Wu, K.-S. Chen, V. K. Sangwan, J. Kang, T. J. Marks, M. C. Hersam, and L. J. Lauhon, Investigation of band-offsets at monolayer–multilayer MoS_2 junctions by scanning photocurrent microscopy, Nano Lett. **15**, 2278 (2015).

[64] J. A. Miwa, S. Ulstrup, S. G. Sørensen, M. Dendzik, A. G. Čabo, M. Bianchi, J. V. Lauritsen, and P. Hofmann, Electronic Structure of Epitaxial Single-Layer MoS_2, Phys. Rev. Lett. **114**, 046802 (2015).

[65] A. Bruix, J. A. Miwa, N. Hauptmann, D. Wegner, S. Ulstrup, S. S. Grønborg, C. E. Sanders, M. Dendzik, A. G. Čabo, M. Bianchi, J. V. Lauritsen, A. A. Khajetoorians, B. Hammer, and P. Hofmann, Single-layer MoS_2 on Au(111): Band gap renormalization and substrate interaction, Phys. Rev. B **93**, 165422 (2016).

[66] W. Jin, P.-C. Yeh, N. Zaki, D. Zhang, J. T. Sadowski, A. Al-Mahboob, A. M. van der Zande, D. A. Chenet, J. I. Dadap, I. P. Herman, P. Sutter, J. Hone, and R. M. Osgood, Jr., Direct Measurement of the Thickness-Dependent Electronic Band Structure of MoS_2 Using Angle-Resolved Photoemission Spectroscopy, Phys. Rev. Lett. **111**, 106801, (2013).

[67] S. Yang, J. Kang, Q. Yue, and K. Yao, Vapor phase growth and imaging stacking order of bilayer molybdenum disulfide, J. Phys. Chem. C **118**, 9203 (2014).

[68] X. Fan, W. T. Zheng, J.-L. Kuo, D. J. Singh, C. Q. Sun, W. Zhu, Modulation of electronic properties from stacking orders and spin-orbit coupling for 3R-type MoS_2, Sci. Rep. **6**, 24140 (2016).

[69] P.-C. Yeh, W. Jin, N. Zaki, J. Kunstmann, D. Chenet, G. Arefe, J. T. Sadowski, J. I. Dadap, P. Sutter, J. Hone, and R. M. Osgood, Jr., Direct measurement of the tunable electronic structure of bilayer MoS_2 by interlayer twist, Nano Lett. **16**, 953 (2016).

[70] S. Iwata, and A. Ishizaka, Electron spectroscopic analysis of the SiO_2/Si system and correlation with metal–oxide–semiconductor device characteristics, J. Appl. Phys. **79**, 6653 (1996).

[71] L. Grązdiel, M. Krzywiecki, H. Peisert, T. Chassé, and J. Szuber, Photoemission study of the Si(1 1 1)-native SiO_2/copper phthalocyanine (CuPc) ultra-thin film interface, Org. Electron. **13**, 1873 (2012).

[72] L. Skuja, M. Hirano, H. Hosono, and K. Kajihara, Defects in oxide glasses, Phys. Status Solidi C **2**, 15 (2005).

[73] H. Imai, K. Arai, H. Imagawa, H. Hosono, and Y. Abe, Two types of oxygen-deficient centers in synthetic silica glass, Phys. Rev. B **38**, 12772(R) (1988).

[74] R. Salh, L. Fitting Kourkoutis, B. Schmidt, and H.-J. Fitting, Luminescence of isoelectronically ion-implanted SiO_2 layers, Phys. Status Solidi A **204**, 3132 (2007).

[75] K. S. Seol, A. Ieki, Y. Ohki, H. Nishikawa, and M. Tachimori, Photoluminescence study on point defects in buried SiO_2 film formed by implantation of oxygen, J. Appl. Phys. **79**, 412 (1996).

[76] C. R. Helms, and E. H. Poindexter, The silicon-silicon dioxide system: Its microstructure and imperfections, Rep. Prog. Phys. **57**, 791 (1994).

[77] A. F. Zatsepin, D. Yu. Biryukov, and V. S. Kortov, Method for the analysis of nonselective spectra of optically stimulated electron emission from irradiated dielectrics, Phys. Status Solidi **202**, 1935 (2005).

[78] A. F. Zatsepin, V. S. Kortov, N. V. Gavrilov, and D. Y. Biryukov, Photoemission and luminescence properties of quartz glass implanted with Cu+ ions, J. Surf. Invest.: X-Ray Synchrotron Neutron Tech., **2**, 450 (2008).

[79] K. R. Knox, S. Wang, A. Morgante, D. Cvetko, A. Locatelli, T. O. Mentes, M. A. Niño, P. Kim, and R. M. Osgood, Jr., Spectromicroscopy of single and multilayer graphene supported by a weakly interacting substrate, Phys. Rev. B **78**, 201408(R) (2008).

[80] K. R. Knox, A. Locatelli, M. B. Yilmaz, D. Cvetko, T. O. Menteş, M. A. Niño, P. Kim, A. Morgante, and R. M. Osgood, Jr., Making angle-resolved photoemission measurements on corrugated monolayer crystals: Suspended exfoliated single-crystal graphene, Phys. Rev. B **84**, 115401, (2011).

[81] P.-C. Yeh, W. Jin, N. Zaki, D. Zhang, J. T. Sadowski, A. Al-Mahboob, A. M. van der Zande, D. A. Chenet, J. I. Dadap, I. P. Herman, P. Sutter, J. Hone, and R. M. Osgood, Jr., Probing substrate-dependent long-range surface structure of single-layer and multilayer MoS_2 by low-energy electron microscopy and microprobe diffraction, Phys. Rev. B **89**, 155408 (2014).

[82] M. Mankos, D. Adler, L. Veneklasen, and E. Munro, Electron optics for high throughput low energy electron microscopy, Surf. Sci. **601**, 4733 (2007).

[83] See Supplemental Material at http://link.aps.org/supplemental/10.1103/PhysRevB.95.235406 for experimental verification of the apparent lack of charging effects on PES spectra in Fig. S3(b).